

Estimation of spatially distributed latent heat flux over complex terrain from a Raman lidar

W. Eichinger^{a,*}, D. Cooper^b, J. Kao^b, L.C. Chen^a, L. Hipps^c, J. Prueger^d

^a Iowa Institute for Hydraulic Research, University of Iowa, 300 Riverside Drive, Iowa City, IA 52242, USA

^b Los Alamos National Laboratory, Los Alamos, NM, USA

^c Utah State University, Logan, UT, USA

^d National Soil Tilth Laboratory, Ames, IA, USA

Abstract

A method is presented in which estimates of evaporation may be made over an area approaching three quarters of a square kilometer, with relatively fine (25 m) spatial resolution, using three-dimensional measurements of water vapor concentration from a scanning Raman lidar. The method is based upon Monin–Obukhov similarity theory applied to spatially and temporally averaged data. Data from the lidar is used to sense the location and orientation of the surface and the location of the water vapor measurements with respect to that surface. Maps of the spatial distribution of evaporation have been produced showing the evaporation rates at regular intervals throughout the day. The method was applied to the SALSA experimental site during the 1997 summer field campaign. The estimates of evaporation rates made during the campaign compare favorably with estimates made using sap flux methods with RMS differences of 18 W/m². While the method has certain limitations, the three-dimensional character of the data allows for the detection of anomalous situations so that analysts may alter the analysis technique or reject the estimates from the affected regions. This information can be used in a wide variety of ways to study the spatial variations in evaporation caused by changes in soil type and moisture content, canopy type and topography. © 2000 Elsevier Science B.V. All rights reserved.

Keywords: Raman lidar; Topography; Sap flux methods; Evaporation; Complex terrain

1. Introduction

Evapotranspiration is one of the critical variables in both the water and energy balance models of hydrologic systems. These systems are driven by conditions in the soil–plant–atmosphere interface, and as such, involve spatially distributed processes. Traditional techniques of measuring evapotranspiration rely on point sensors to collect information which are often averaged over a region, or assumed to be representative of a far larger area. Spatially averaged data from point sensors near the surface are limited in value because of

the relatively small footprint size which an individual point sensor represents, the necessarily limited number of sensors which are used to make the measurements, and because of our current inability to extend the measured values at a point (or series of points) to an understanding of the processes that are occurring on larger scales. Part of the problem is that the bulk of the earth's surface is not horizontally homogeneous with respect to topography, soil moisture availability, soil type, or canopy. Eddy correlation has been successfully used from aircraft to cover large areas, but the usefulness of the data has been called into question for use in mixed canopies where spatially resolved fluxes are desired (e.g., Mahrt, 1998).

* Corresponding author.

Remotely sensed data has the potential to provide detailed information over a relatively large area with high spatial resolution. Examples include thermal sensing of the surface where the latent heat flux is determined as a residual in the energy balance (e.g., Jackson et al., 1987) or two-dimensional water vapor concentrations from ground or airborne lidar (e.g., Ehret et al., 1993; Higdon et al., 1994). The problem then is to develop methods by which evaporative energy fluxes, may be reliably inferred from the types of information that current remote sensors can provide.

The three-dimensional scanning Raman lidar built by Los Alamos National Laboratory can provide detailed maps of the water vapor concentration in three dimensions with high spatial and temporal resolution. Using this information, a methodology has been developed to estimate the spatially resolved evaporative flux over the scanned area. The ability to determine evaporative fluxes has been previously demonstrated over ideal surfaces, i.e., flat, uniform terrain and canopy (Eichinger et al., 1993a,b). We describe our ongoing efforts to extend that capability to mixed terrain and canopies in conjunction with the SALSA 1997 intensive field campaign.

The Semi-Arid Land Surface Atmosphere (SALSA) Program studies basin-wide water balances, its changes and the resulting effects on the ecology of semiarid regions. The study has centered on the San Pedro River basin which crosses the border between the United States and Mexico to the east of Tucson, AZ. The 1997 summer field campaign centered on that part of the river in the Lewis Springs riparian corridor 5 miles east of Sierra Vista, AZ. Extensive measurements were made of the ground and surface water levels, energy fluxes and plant transpiration using a wide variety of instruments as well as supporting aircraft and satellite measurements. The site consists of a cottonwood stand in the immediate vicinity of the river with sacaton grass and mesquite surrounding. The site provides an especially difficult test for the measurement of spatially resolved fluxes in that all three canopy types are mixed. Within the region that the lidar can observe, there are large variations in surface elevation and types of canopy, making the canopy top highly irregular. The day chosen for intercomparison is one in which all of the required instruments worked properly and which represented a “typical” day, not necessarily one that was meteorologically

logically “best” (attempting to maximize the amount of fetch over the cottonwoods).

2. Instrument description

The solar-blind Raman water vapor lidar used in these experiments is based upon the Raman technique pioneered by Melfi et al. (1969) and Cooney (1970) and extended for daytime, solar-blind operation by Renault et al. (1980), and Cooney et al. (1985). The device operates by emitting a pulsed ultraviolet laser beam into the atmosphere. Raman scattered light from nitrogen gas and water vapor is collected by the telescope on the lidar and converted to an electric signal. The system operates in the solar-blind region of the spectrum using krypton fluoride as the lasing media to obtain light at 248 nm. The Raman-shifted nitrogen signal returns at 263 nm and the Raman-shifted water vapor signal returns at 273 nm. Simultaneous measurement of the water vapor and nitrogen returns provides a simple method for obtaining absolute measurements. Because nitrogen is, by far, the most abundant atmospheric gas, dividing the Raman-shifted return signal from water vapor by that of nitrogen normalizes each pulse and corrects for first-order atmospheric transmission effects, variations in laser energy from pulse-to-pulse, and telescope field-of-view (FOV) overlap with the laser beam. The divided returns are then proportional to the absolute water vapor content of the air. A correction is required to account for the differential atmospheric attenuation between the nitrogen and water vapor wavelengths.

The typical maximum horizontal range for the lidar is approximately 700 m when scanning, with a corresponding spatial resolution of 1.5 m over that distance. The upper scanning mirror allows three-dimensional scanning in 360° in azimuth and $\pm 22^\circ$ in elevation. The uncertainty in the water vapor mixing ratio is typically measured to be less than 4%. Details of the instrument, data collection, and determination of water concentration may be found in Eichinger et al. (1999).

3. Lidar derived flux method

The water vapor concentration in the vertical direction can be described using Monin–Obukhov

similarity method (MOM) (Brutsaert, 1982). With this theory, the relationships between the properties at the surface and the water vapor concentration at some height, z , within the inner region of the boundary layer is

$$q_s - q(z) = \frac{E}{L_e k u_* \rho} \left[\ln \left(\frac{z}{z_{0v}} \right) + \psi_v \left(\frac{z}{L} \right) \right] \quad (1)$$

where the Monin–Obukhov length, L , is defined as

$$L = - \frac{\rho u_*^3}{kg[(H/Tc_p) + 0.61E]} \quad (2)$$

where z_{0v} is the roughness length for water vapor, q_s and T are the surface specific humidity and temperature, $q(z)$ the specific humidity at height z , H the sensible heat flux, E the latent heat flux, ρ the density of the air, L_e the latent heat of evaporation for water, and u_* the friction velocity (Brutsaert, 1982), k the von Karman constant, taken as 0.40, and g the acceleration due to gravity. ψ_v the Monin–Obukhov similarity function for water vapor and is calculated as

$$\psi_v \left(\frac{z}{L} \right) = 2 \ln \left[\frac{(1 + x^2)}{(1 + x_{0v}^2)} \right] \quad (3)$$

where

$$x = \left(1 - 16 \left(\frac{z}{L} \right) \right)^{1/4} \quad (4)$$

for unstable conditions, and where x_{0v} represents the function x calculated for the value of z_{0v} . The roughness length is a free parameter to be calculated based upon the local conditions. Heat and momentum fluxes are often determined from measurements of temperature, humidity, and wind speed at two or more heights. These relations are valid in the inner region of the boundary layer where the atmosphere reacts directly to the surface. This region is limited to an area between the roughness sublayer (the region directly above the roughness elements) and below 5–30 m above the surface (where the passive scalars are semi-logarithmic with height). The vertical range of this layer is highly dependent upon the local conditions. The top of this region can be readily identified by a departure from the logarithmic profile near the surface. Fig. 1 is an example of a water vapor profile with a logarithmic fit showing such a departure at approximately 4 m above the surface. Suggestions have been made that the atmosphere is also logarithmic to higher levels and may integrate fluxes over large areas (Brutsaert, 1998). This assertion is intended to be the subject of future investigation.

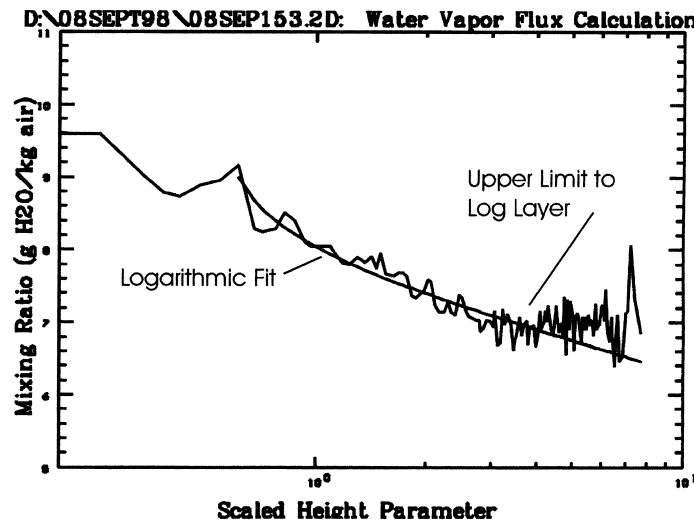


Fig. 1. An example of a vertical profile of the water vapor concentration determined by the lidar. A logarithmic fit is also shown. Note the break in the slope of the water vapor concentration at approximately 4 m. The location of this break is taken as the height of the top of the inner region of the boundary layer. The height of this break ranges from a few meters to about 30 m.

Evaporative fluxes have previously been obtained from a combination of Monin–Obukhov similarity theory and vertical water vapor profiles taken with the lidar (Eichinger et al., 1993b). In these initial efforts, the correlation between the lidar and eddy correlation was good, with regression statistics of an r^2 of 0.73 and an RMS difference of about 12% of the eddy correlation value. A single scan that required as much as 30 min to complete was used in the previous estimates whereas two or more scans requiring 30–45 s each are averaged in this work. It was noted in the initial work that multiple measurements averaged over time produced more reliable estimates of the evaporative flux.

The present method used begins by rearranging (1) into a linear form

$$q(z) = -Mz' + c \quad (5)$$

where M is the slope of the fitted function ($M = E/(L_e k u_* \rho)$), z' is a reduced height parameter ($z' = \ln(z - d_0) - \psi_v((z - d_0)/L)$), and c is a regression constant ($c = M \ln(z_0) + q_s$). Measurements for the slope are made based upon a least squares fit to several hundred measurements of water vapor concentration. Having determined M from the slope of the fitted line, the flux is then

$$E = L_e M k u_* \rho \quad (6)$$

where u_* and L are obtained from local measurements.

Previous work to obtain evaporative fluxes from the lidar was done over sites that were level and in which the geometry between the lidar and the canopy top was well known. Thus the sites were ideal in that they were horizontally homogeneous, but also in that the height of a particular lidar measurement above the canopy was easily and well determined. Thus it would be expected that this technique should reproduce fluxes as measured by other techniques. Gradient methods for determining fluxes are well established (Stull, 1988; Brutsaert, 1982). The lidar method is unique in that it uses a large number of measurements to determine the vertical water vapor gradient. The extension of the method to rough terrain presents issues relating to assumptions of horizontal homogeneity as well as the determination of the surface location (with respect to the lidar) and the direction of the normal to the surface.

Fig. 2a is a typical scan from the Raman lidar showing the water vapor concentration in one vertical plane

at the SALSA-MEX site. The intense red color at the bottom is a result of the attenuation of the laser beam by the ground, bushes, or trees and by the fluorescence of the organic compounds in the canopy. The attenuation of the laser beam reduces the intensity of the nitrogen and water vapor signals, but fluorescence increases the intensity of the water vapor signal at 273 nm relative to the nitrogen signal at 263 nm. Since the water vapor concentration is found from the ratio of the two signals, the algorithm produces an apparent large water concentration inside plant canopies. While the values are spurious, they are useful in identifying the canopy surfaces. Fig. 2b is a conceptual drawing showing the site and how the various lidar lines of sight are used to scan the area and produce the first figure. For this experiment, the lidar had a nominal 1.5 m range resolution. In other words, at every 1.5 m along each of the lines shown in Fig. 2b, a measurement of the water vapor concentration was made. Each of these measurements is used to build up a two-dimensional plot of water vapor concentration. The SALSA-MEX site is far from ideal in the sense that it is not horizontally homogeneous and the height above the canopy of a given measurement varies considerably and is not dependent upon geometry alone.

The flux estimation method used assumes that in some region, taken for this experiment to be 25 m in size, but may be any user selected value, the slope of the water vapor concentration in the z -direction can be determined from a curve fit using all of the measurements of the water vapor concentration above that region. This assumes horizontal homogeneity inside the region and with the region immediately upwind, that the aggregate of the values constitutes a measurement of the average condition over the region, and that the slope in water vapor concentration is the result of conditions inside that region. The limitations of these assumptions will be discussed later.

A key capability of the lidar that is useful in estimating fluxes over complex terrain is the ability to determine the location of the surface. The lidar at the SALSA experimental site was sited so that it looked down on even the cottonwoods and was thus able to determine the location of the surface for all of the canopy types. For the case of mixed terrain and canopy, the lidar is used to find the location of the surface in the range interval under investigation. Fig. 3 is a conceptual drawing of how this is accomplished. The top of

8/11/1997 14:00 VLaserPulses=100 Az: 60.00 Elev: -4.50; Vertical Scan Right Hand limit of View

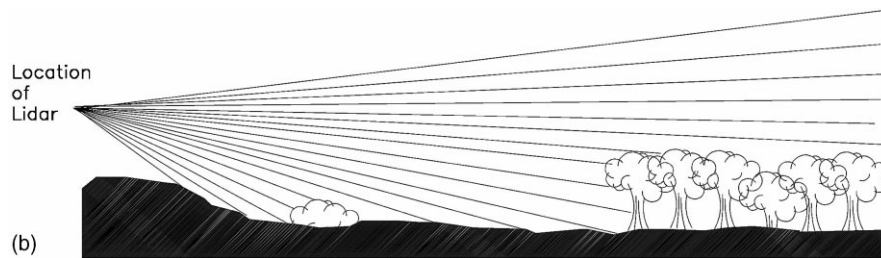
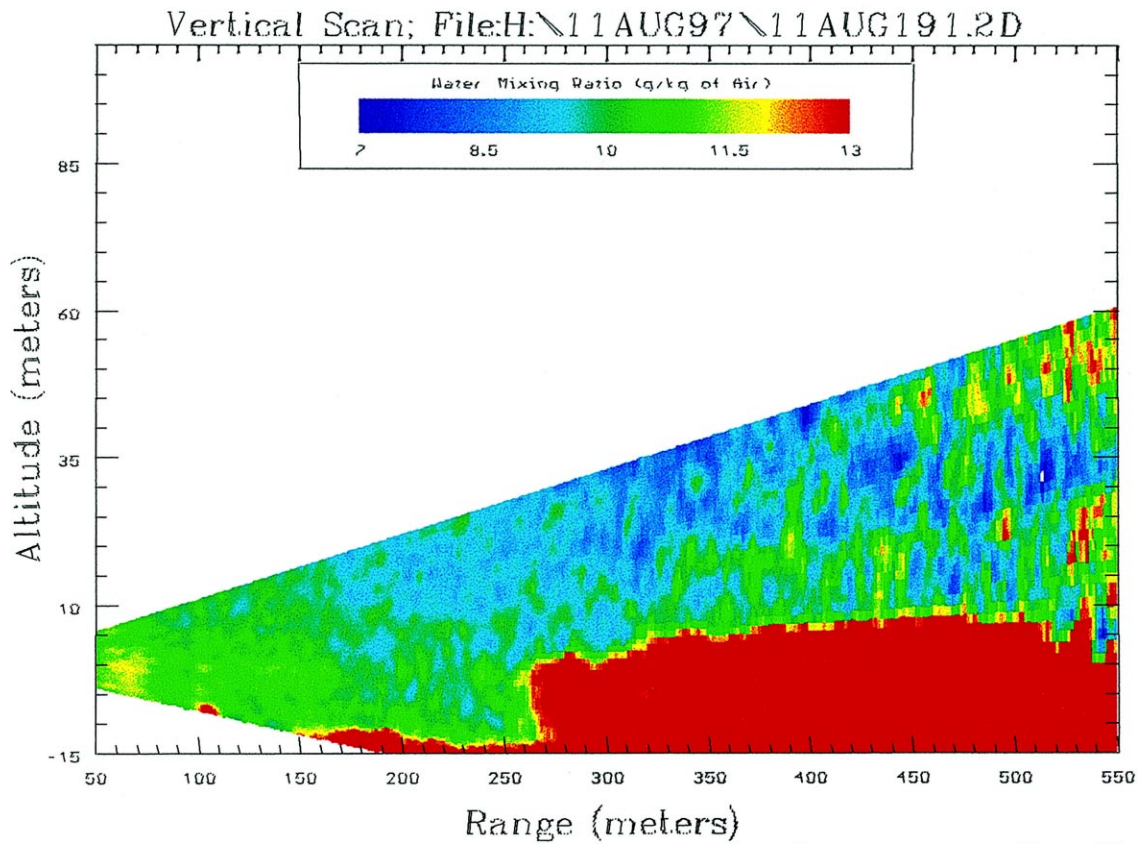


Fig. 2. (a) A vertical scan from the lidar showing the water vapor concentrations in a vertical plane at the SALSA site. Red colors represent highest water concentrations and blues represent the lowest concentrations. (b) A conceptual drawing showing the SALSA site as shown above and how different lines of sight from the lidar are combined to make the water vapor concentrations map. The water vapor concentration is determined every 1.5 m along each of the lines shown. The lines of sight in actual practice are 0.15–0.25° apart.

the canopy is found either from the abrupt change in the apparent water concentration or from the abrupt change in the elastic lidar signal which is also recorded along each line of sight. The location of the top of the canopy as a function of distance is determined using

multiple lines of sight. A linear least squares fit is made to determine the elevation and slope of the top of the canopy within the range interval under consideration.

For an individual water vapor measurement, the distance from the measured point to the surface along a

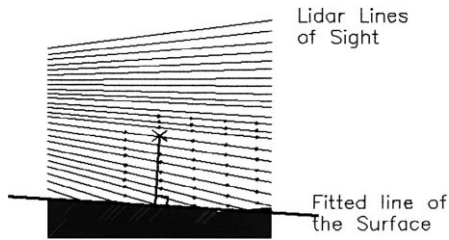


Fig. 3. A conceptual drawing of a 25 m region and all of the lidar lines of sight within it. The location of a line approximating the surface is determined, and the distance from each measured value to this line along a perpendicular to the line is calculated. All of the measured values of water vapor concentration are used in the calculations shown in Fig. 3.

line perpendicular to the measured slope and elevation is used as the corrected height above the surface (see Fig. 3). This means that the z -direction is taken to be the direction perpendicular to the canopy top and not the vertical gravitational direction. The reasoning is that, near the surface, the flow of air will be parallel to the local surface and that dispersion of the water vapor released from the surface in the direction perpendicular to the mean flow is most important to the estimation of evaporation (Kaimal and Finnigan, 1994).

For an individual scan, all of the measurements within a region are used to estimate the slope of the single line described by Eq. (5). Fig. 4 is an example of such a fit to data from Fig. 2a. All of the water vapor measurements in the region between 200 and 225 m from the lidar have been included and used to fit a

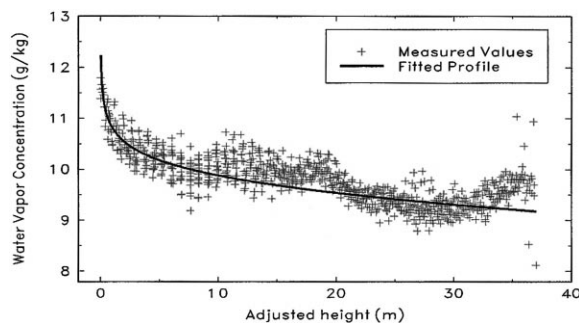


Fig. 4. An example of a lidar fitted vertical profile and the data from which it was calculated. The data is from 200 to 225 m from the scan shown in Fig. 1a. The relatively large variability in the data about the fitted line is due to the presence of discrete structures. If a large enough area is averaged, the mean value at each elevation converges to a logarithmic profile.

logarithmic profile. While there is considerable spread in the measurements at each height above the ground, the slope is statistically measured to an uncertainty of 1.2% for this case. The spread in the measurements are due to the existence of coherent structures containing high and low water vapor concentrations. These structures can be seen in the two-dimensional plots (e.g., Figs. 2, 8a and b).

A measured value of the Monin–Obukhov length is used to further adjust for atmospheric stability. However, in practice, the use of this correction results in a small (usually on the order of 5% or less) change in the estimated flux. A severe limitation of this method is the lack of a u_* measurement for each 25 m region. In the ideal case, we divide the region into surface types and use a measured u_* typical of that region. For the SALSA experiment, there were a grass region, a mesquite region, and a forested region. The u_* values over the grass and mesquite were determined using three-dimensional sonic anemometers. The u_* values used in determining the flux in the riparian corridor were derived from wind data taken immediately adjacent to the zone.

The fractional uncertainty of the lidar flux measurements were estimated using

$$\frac{\delta E}{E} = \left[\left(\frac{\delta u_*}{u_*} \right)^2 + \left(\frac{\delta M}{M} \right)^2 + \left(\frac{\delta \rho}{\rho} \right)^2 + \left(\frac{\delta q}{q} \right)^2 \right]^{1/2} \quad (7)$$

where δu_* , δM , δr , and δq are the uncertainties in the u_* , slope, air density, and water vapor concentration measurements, respectively (Bevington and Robinson, 1992). The last term on the right is a contribution from a systematic uncertainty (or bias errors) in the lidar measurement of water vapor. While an individual measurement may be uncertain to the 3–4% level (a measure of the precision error), the determination of the mean concentration from a number of measurements (a measure of the bias error) is more accurate. This contribution is determined by the calibration error of the instrument and is a function not only of the lidar, but also of the instrument(s) used to calibrate the lidar. For this reason, calibration is done with instruments traceable to the US National Institute of Standards and Technology (NIST). As the range increases, the precision of the lidar degrades because of the r -squared fall off in the signal, but the mean value

of the measurements is maintained. Thus the variation in the data about the fitted line is generally observed to increase with distance, but since the mean value of the measurements is maintained, this should have a minimal effect upon the slope measurements and thus the estimated flux. The bias error in the mean value is taken to be less than 2%.

The value of the slope can be estimated with high certainty due to the large number of measurements used in fitting Eq. (5). The nominal uncertainty in the value of the slope is 1–2%. The air density is obtained from local measurements of temperature and air pressure. The uncertainty in the value of the air density is much less than 2%. The value of the surface wind stress u_* is normally the primary source of uncertainty, normally ranging from 5 to 15%. The value of the uncertainty of u_* is a function of the uncertainty in the measurements of u_* at a given point, but also contains a contribution from the assumption that a measurement at one point may be applied to a similar surface some distance away (the magnitude of which is highly site specific). The uncertainty in a measurement of u_* is difficult to assess. While uncertainty estimates based upon the accuracy of the anemometer wind measurements result in estimates on the order of 5%, two anemometers a meter apart in ideal conditions may have u_* values that differ by as much as 35% (although typical values are generally much less). For a typical measurement of the evaporative flux, the total uncertainty is determined almost totally by the uncertainty in u_* and leads us to estimate an overall uncertainty on the order of 15%. For areas far from u_* measurements, the uncertainty may be as much as twice as large.

Fig. 5 is a comparison of the latent heat flux measurements from sap flow gages in the cottonwoods (Schaeffer and Williams, 1998) made throughout a day and in the same region as estimates from the lidar. Details of the sap flux measurements can be found in the paper in this issue. The two evaporation estimates track well through the day. These data compare with an r^2 of 0.89 and an RMS difference of 18 W/m^2 . One would expect a small bias error due to soil evaporation that is not measured by the sap flux instruments. It may be that the soil evaporation component is smaller than the relative uncertainties (about 20 W/m^2), and much smaller than the transpiration so that this effect is not apparent.

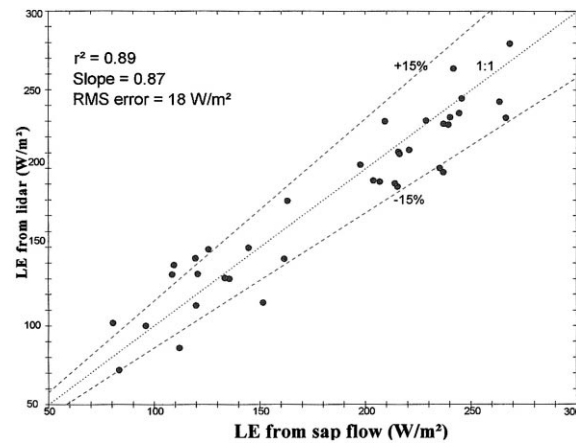


Fig. 5. An example of a comparison of the lidar evaporation estimates throughout a day made in the same region as sap flux measurements made in the cottonwoods. The two estimates track well through the day with an r^2 of 0.89 and an RMS difference of 18 W/m^2 . The slope of the best fit line is 0.87.

4. Areal evaporation estimates

In making a measurement over a the site, the locations of special interest, such as the location of supporting sensors, and the size of the area to be examined are determined. The azimuths to locations deemed critical are determined and a scan pattern is developed. The scan pattern is then adjusted to cover the area as evenly as possible and as often as possible and at least twice per half hour. As noted in the first efforts to develop the method, increasingly precise estimates are obtained when multiple estimates are averaged at each location. Because of the finite time required to make an individual measurement (between 30 and 60 s to make a single vertical scan), there is always a conflict between the need to cover as large an area as possible with as fine a horizontal resolution as possible with the desire to repeat each scan as many times as possible.

Implicit in the similarity technique is the assumption that the values measured represent the average condition. While spatial averaging can, to some extent, substitute for temporal averaging, the use of a 25 m spatial extent cannot fully capture all of the larger scale events. Thus the scan pattern repeats the measurement as often as possible. In a 30 min averaging period, we have taken two measurements along each azimuth line as the minimum acceptable. At long ranges where the measurements are separated by larger differences in

the azimuthal direction, this gives at least two measurements in each 25 m bin. At closer ranges, where there may be several azimuth lines through each 25 m square, considerably more evaporation estimates are averaged. This averaging improves the evaporation estimates. The more estimates averaged, the better the result, particularly during transitions when the wind speed or direction is changing.

The use of a more limited number of lines of sight (i.e., increasing the size of the angle between lines of sight in the vertical direction) has been investigated. A profile could be constructed from as few as three lines of sight in the vertical direction which would enable scanning of a larger area and each line of sight could be revisited more often. However, for areas which are unusually non-homogeneous, this would result in a great deal more uncertainty as well as the loss of the ability to determine the cause of anomalous fluxes and to adjust the analysis accordingly. The fine angular resolution used here enables the precise determination of the location of the canopy top and its slope. The large number of lines of sight and data also serves to average the effect of coherent structures on the vertical gradient. Less data would increase the impact that these structures have on the estimated flux. A key part of the analysis is the estimation of the maximum height of the data that can be used in the determination of the gradient. This height is found by determining the altitude at which the slope changes. With less data, this would be more difficult and less accurate. Lastly, as will be discussed in the next section, there are situations in which the atmosphere is not well behaved and causes the estimated fluxes to be wrong. The visual two-dimensional plots are a great tool in determining when and where these situations may occur and if the analysis method can be modified to produce a more correct estimate.

The analysis methodology described above is executed along each azimuth angle for each incremental distance. As will be noted in the next section, occasionally evaporation values will be produced that are clearly non-physical. These values are used to trigger a manual analysis and are usually caused by some anomaly. Within each 25 m cell, all of the data values are averaged. Any of a number of plotting packages can be used to create contours from the data. Fig. 6 shows a comparison of an areal evaporation map with a canopy map. The two maps correspond in that the lowest evaporation rates are found in the grassy area,

medium rates in the mesquite, and the highest rates along the river in the cottonwoods. There is a long area that is predominantly grassland about 200–400 m due south of the lidar in which the evaporation rate is abnormally high for the grass and scrub found there. However, this region is significantly lower in elevation than the surrounding area, being nearly at the level of the river. A shallow water table in this area may account for the excess evaporation. Since the height of the ground surface cannot be determined for the areas on the far side of the woods from the lidar, the evaporation estimates generated by the program for the grass area west of the woods (left side of the plot) are not reliable.

5. Limitations of the method

The method used here to develop maps of the evaporative flux in complex terrain assumes that, in some small region, the slope of the water vapor concentration in the direction perpendicular to the surface is governed by Monin–Obukhov similarity theory. This assumes horizontal homogeneity inside the region and to the region immediately upwind, that the aggregate of the values constitutes a measurement of the average condition over the region, and that the slope in water vapor concentration is the result of conditions in that region.

Clearly in transition areas where the canopy type or groundwater availability changes dramatically, the method will have problems. For example, the area immediately downwind of the wooded area consistently gives estimates that are unreasonably high or low. The vertical scans shown in Fig. 7a and b are examples of situations in which a “plume” of moist air extends from the upper reaches of the wooded area over the mesquite. This will certainly bias the measurement of the slope if this situation continues to persist over several scans since it produces a substantially higher water vapor concentration at altitude above the mesquite.

One of the implicit assumptions of Monin–Obukhov similarity theory is that transient events are averaged into the mean. In the situation where a plume of moist air is transported from the trees, the assumption is not valid and a modified profile would be required. For cases such as those shown in Fig. 7a and b, the data is manually processed to include only data from a much

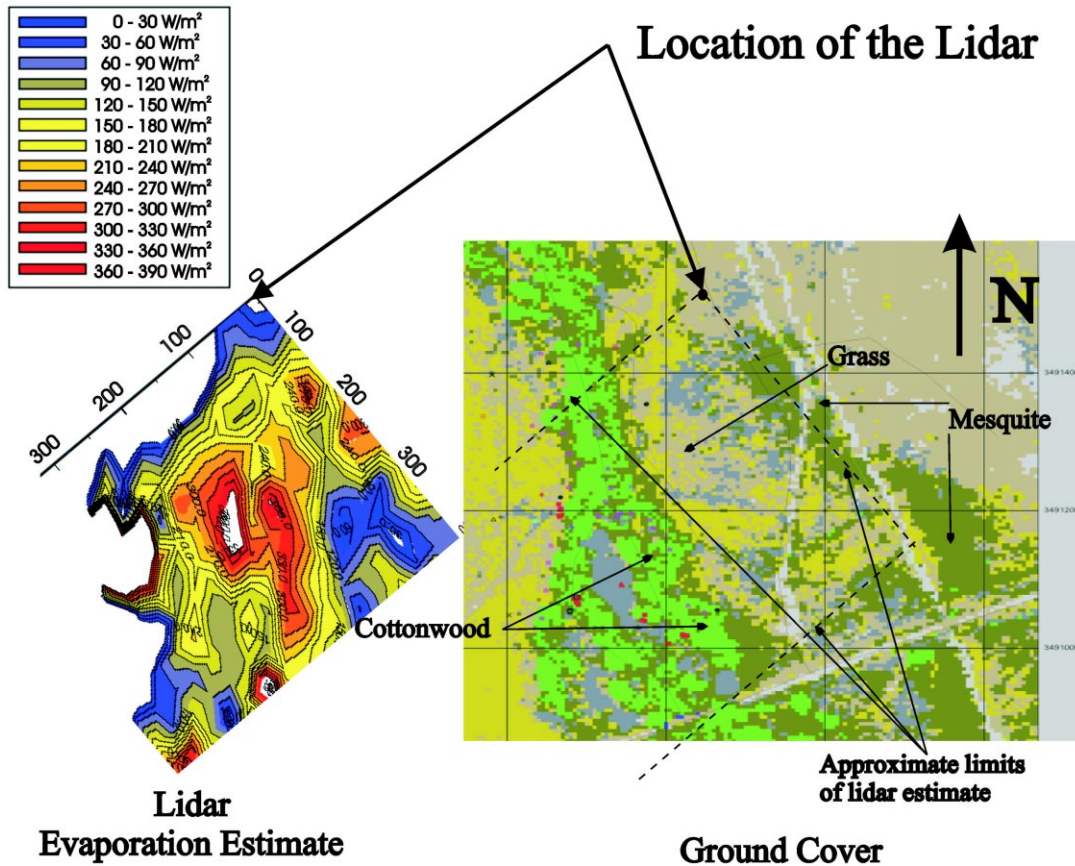


Fig. 6. An example of a map of the evaporative flux determined by the method described for the 13:00–13:30 h time period. Also shown is a map of the canopy cover over the same region to approximately the same scale. Note that evaporation rates are highest near the river, in the trees and lowest in the grassy areas. The grid lines on the canopy map are 200 m apart. The distances in meters are also marked on the evaporation map.

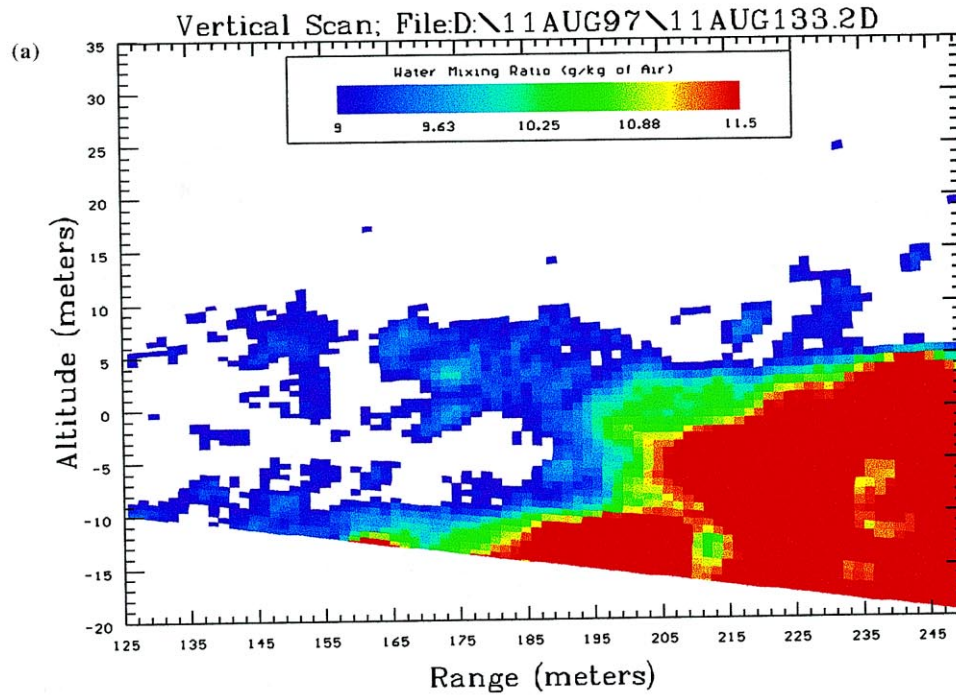
shorter distance above the canopy where the anomaly has less effect on the mean slope of the profile. This reduces the total number of points used to determine the slope by a factor of about three, but produces evaporation estimates that are more realistic.

Also at issue in transition regions is the issue of the location of the surface when the canopy is discontinuous. An example is shown in Fig. 2a at a distance of 270 m from the lidar. This is the edge of the wooded area. At this point, the location and slope of the canopy top are meaningless quantities with respect to this analysis methodology. If the canopy change is not abrupt, but changes smoothly and the water vapor concentration is examined perpendicular to the slope of the surface as described above, the water vapor con-

centration with height is observed to be logarithmic. How the atmosphere changes at abrupt changes in the surface is currently the subject of further investigation.

Conditions occur near areas of transition in which moist areas upwind alter the water vapor concentration near the surface so that it is not logarithmic in z . When this occurs, the methodology just described in this paper cannot be used. Fig. 8c is an example of the water vapor released in the cottonwoods increasing and changing the water vapor concentration above nearly a 100 m area and nearly all the way down to the canopy. When this occurs, the flux estimation method seldom produces evaporation estimates that are unreasonable and thus this condition can be found only by visual examination of the vertical scans.

8/11/1997 12:29 #LaserPulses=100 Az: 40.00 Elev: -4.50; Vertical Scan Right Hand limit of View



8/11/1997 11:39 #LaserPulses=100 Az: 85.00 Elev: -4.50; Vertical Scan

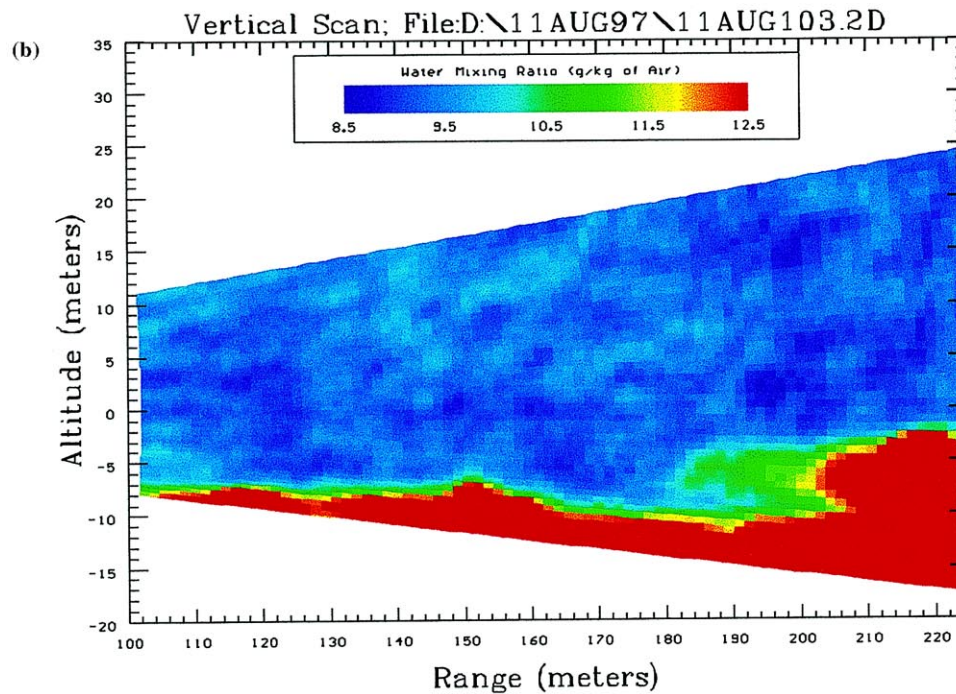


Fig. 7. Two vertical scans from the lidar showing the “plumes” of water vapor coming from the cottonwood trees upwind. These plumes affect the determination of the slope of the water vapor concentration in the vertical direction.

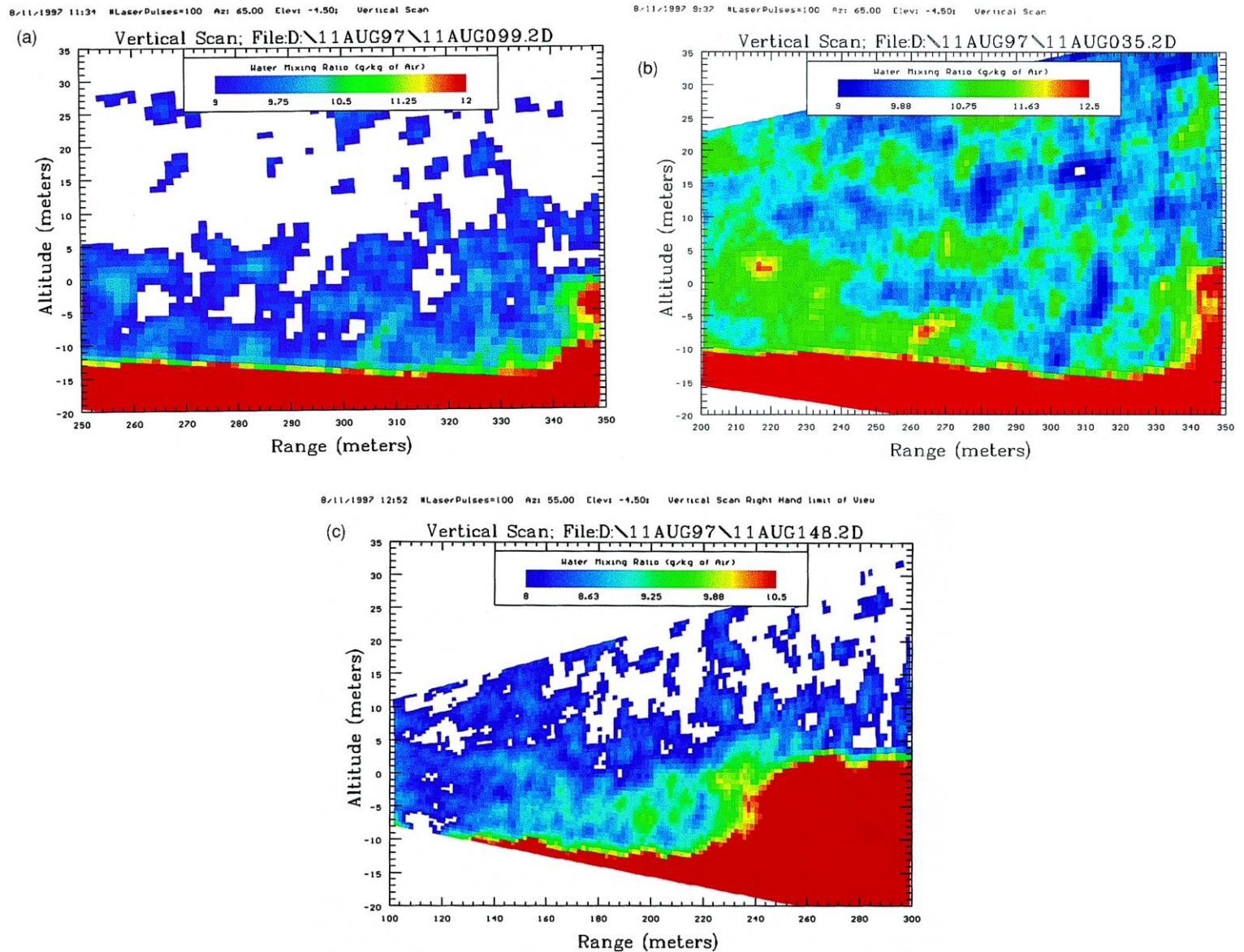


Fig. 8. (a) A vertical scan from the lidar showing the normal condition with discrete water vapor structures over the canopy. Despite the existence of these structures, the average condition converges to a logarithmic form for large enough areas. (b) A vertical scan showing a situation in which a discrete water vapor structure (at approximately 260 m from the lidar) has sufficient concentration to alter the average so that it does not converge to a logarithmic form. No alternative analysis is currently available for such a condition. (c) A vertical scan showing a situation in which the plume from the cottonwoods extends far enough downwind and down to the canopy. For this condition, the water vapor concentration over the canopy downwind of the trees is not representative of that canopy and cannot be used to estimate an evaporation rate.

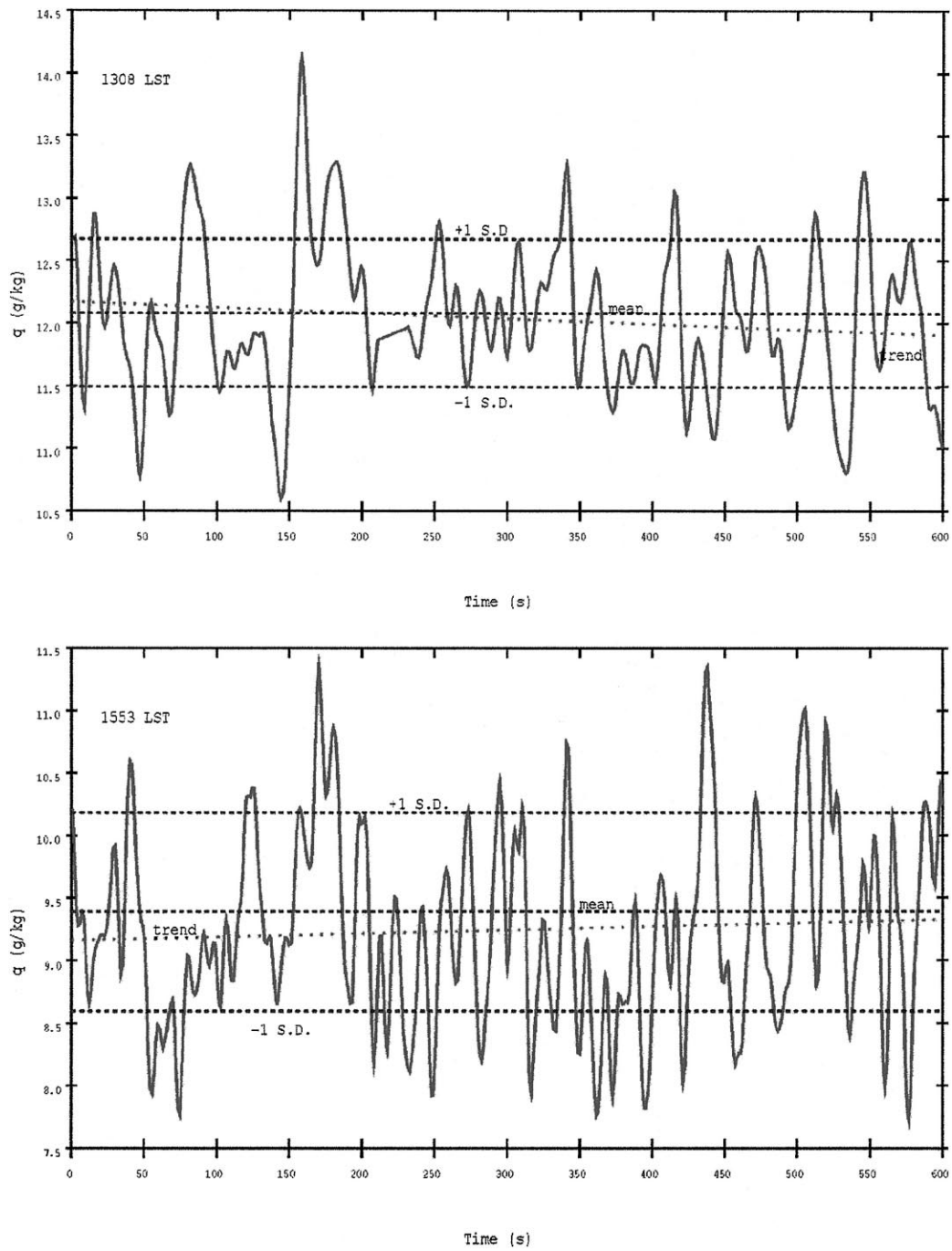


Fig. 9. The water vapor concentration at two separate times in the afternoon showing the variations with time. Also shown are the average and least squares linear fits to the data.

In complex terrain, changes in the canopy lead to changes in the evaporation rate which lead to changes in the water vapor concentration along the surface. Because of advection, these changes may result in flux divergence, particularly in the vertical direction $\partial w'q'/\partial z$. One may estimate the size of this term from the size of the $\bar{u}\partial\bar{q}/\partial x$ and $\partial\bar{q}/\partial t$ terms in the conservation equation for water vapor. It is not uncommon to find horizontal gradients in water vapor concentration of -0.2 g water/kg air in a 25 m analysis region downwind of the riparian area. When offset by a small increase in water content over the same period of time (see Fig. 9), this leads to a potential flux divergence of about 50 W/m² per meter of height above ground. At this time, the effect of advection on the Monin–Obukhov flux method is unknown, but is a subject of current research. We note that the corrections due to non-stationarity are, in general, small. From Fig. 9, we can see two examples of the water vapor concentration at a given range over time with the average value and the least squares linear fit also shown. The change in water concentration over a 10 min period is approximately 0.3 – 0.4 g water/kg air. This results in a correction of less than 5 W/m².

Related to the question of advection is the question of the location of the source (also known as the footprint) for a measurement at a given height. This is a subject of considerable current interest (e.g., LeClerc and Thurtell, 1990; Horst and Weil, 1994; Finn et al., 1996; Horst, 1999). More than two-thirds of the measurements used in any given profile are below 8 m. On more than half of the profiles, the maximum height used is 8 m or less. The greatest curvature in the profile is found at heights less than 4 m, and it is those measurements less than 4 m that play the greatest role in determining the slope of the line. The Monin–Obukhov lengths for the day used in the analysis were on the order of -20 m. Using the methodology outlined by Horst and Weil (1994), one can estimate the upwind distance contributing to the flux at a given height. For a height of 8 m, the upwind distance, past which less than 20% of the flux is generated, is a factor of approximately five times the measurement height, or about 40 m. This would tend to indicate that the bulk of the flux in a given 25 m section is generated inside that section and the section immediately upwind. Thus it would be prudent to recognize that the flux locations as given by the

methodology are not exact, but rather are somewhat diffuse in the upwind direction. In practice, this has not been an issue in that the estimated fluxes do not show many instances of large, abrupt changes.

Also related to the subject of advection is the question of the ability of the lidar to resolve structures in the vertical lidar images even when there is substantial time elapsed between the start and finish of the scan. In the case of the SALSA data we can estimate the Lagrangian time scale T_L , which, according to Kaimal and Finnigan (1994), is a “measure of the persistence of the turbulent eddies” as $T_L = 0.33h_c/\sigma_w$, where h_c is the height of the canopy, and σ_w is the standard deviation of the vertical wind speed, w , at h_c . In the context of lidar-imaged structures, if the time required to complete that part of the lidar scan containing the structure is less than T_L , then the structures observed will have statistical properties that are representative of the true atmospheric turbulence and the image distortions due to “slow” scanning will not be significant. For a structure with a size on the order of 15 m, it will take 4–6 s for the lidar to scan over its volume with the entire scan requiring approximately 30 s to complete. The canopy height was approximately 15 m and σ_w (measured by sodar) ranged from 0.4 to 0.75 m/s during the day. Thus the estimated structure lifetime is expected to range from about 7–12 s. While the total time required to complete a given vertical scan is on the order of 30 s, the time required to image a coherent structure is much shorter, and considerably shorter than a typical structure lifetime. Thus, while one may expect significant distortion of the entire image from movement and evolution of the structures during the time required to make a scan, one would expect that the scanning speed is fast enough to capture the individual structures. Clearly, a faster scanning speed is desirable; the development of that capability is currently an area of emphasis. As with most lidars, there is a trade-off between maximum effective range and the speed with which a scan may be completed. We expect that competition between these two goals will always be an issue.

There remains the question of how well the measurements averaged over distances as short as 25 m and less than a minute in time represent the average conditions. An individual scan will often show structure near the surface. An example is shown in Fig. 8a. In most cases, this will produce deviations

above and below the average value, but which average to profiles that are logarithmic. Occasionally there are plumes that contain water vapor concentrations that are significantly higher than normal. In such cases, as for example shown in Fig. 8b, the profiles are significantly altered and may no longer be logarithmic. At present, when such events as the plume at 260 m in Fig. 8b are found, the evaporation estimate from that 25 m section is discarded. No analysis method has been found which can incorporate such structures to produce an evaporation estimate. A more detailed analysis of the structure of the water vapor concentrations and fluxes is presented in Cooper et al. (1999).

In using this method for determining fluxes, the optimal maximum height for inclusion of the water vapor measurements must be determined. This corresponds to the height of the change in slope shown in Fig. 1. While the largest possible distance over which the measurements are made leads to the greatest accuracy, measurements too close to the surface or so high that they are outside the inner region lead to erroneous estimates of the water concentration gradient. This height varies throughout the day so the method for determination must be dynamic and adjust to the existing conditions. In this analysis, the same height has been used over all of the canopy types, but the possibility exists that different heights would be appropriate over different canopies.

While limitations of the method exist, the amount and type of data provided by the lidar allows one visually to determine what is happening at a particular location that causes the estimates to be anomalous. The existence of visual two-dimensional information that allows one to correct for unusual circumstances is a very powerful asset and offers the potential for improved algorithms which may overcome the deficiencies in the current formulation. At present, these conditions require the intervention of a human analyst to determine the proper method of analysis to be made. This methodology must be highly automated if it is to be truly efficacious. Work continues to accomplish this.

6. Conclusion

Maps of the spatial distribution of evaporation have been produced using spatial water vapor concentra-

tion data from a scanning Raman lidar. The estimates of evaporation rate compare favorably with other estimates made using other methods. The method developed allows estimates of the evaporation rate to be made with relatively small (25 m) spatial resolution over an area approaching three quarters of a square kilometer. As much as 25–40 MB of data are analyzed to generate each flux map. Because of the amount of data and time required to perform the analysis, methods and criteria are currently under development to automate the entire analysis process over all of the azimuthal angles for a given averaging time period. Criteria are being developed to flag and ignore data that do not converge to a logarithmic profile and to not include data above the internal boundary region in the analysis. Automation of the analysis will allow near real time determination of the evaporation estimates.

While there are significant limitations to the method, it remains a relatively direct method of estimating the fluxes in situations where conventional methods fail or when the topography makes it difficult to site instruments or field enough of them to achieve an areal average. A major limitation is related to changes in the topography, and how much of the atmosphere above a given site can be considered to be influenced by the surface and thus used to estimate the flux in that region. An advantage of this method is that the spatial water vapor measurements themselves can be used to determine the regions in which these problems may occur. The large number of water vapor measurements used to determine the slope also make it possible to determine where the slopes change and thus limit the maximum height of the water vapor measurements used to determine the slope.

Efforts are currently underway to improve the range of the lidar system by increasing the photon efficiency of the system. This will make it possible to scan faster so that more scans can be repeated over a larger area. Efforts are also being made to add the ability to measure spatially resolved temperature using a Raman technique (Nedeljkovic et al., 1993). The addition of temperature will allow determination of the partitioning of solar energy between sensible and latent heat fluxes using similar methods. The ability to estimate these fluxes in a spatial manner will enable progress in a number of fields which examine the role that the canopy plays in partitioning solar energy. On a longer time frame, methods are being examined that may

allow the lidar to perform eddy covariance measurements along a single line of sight.

The method used here can provide reliable estimates of the evaporation rate over a relatively large area with relatively fine spatial resolution. The method is a more direct method of estimating the fluxes than most remote sensing techniques that estimate the evaporation rate as a residual. It also provides regular estimates throughout the day as opposed to intermittent satellite or aircraft measurements. This information can be used in a wide variety of ways to study the spatial variations in evaporation caused by changes in soil type and moisture content, canopy type and topography. Because of the extensive nature of the estimates in space and time, evaluation of the relative contributions of each of these can be determined. The type of measurements provided also provide the opportunity to span the scales between the footprint of point measurements and the kilometer scale measurements made by satellites.

Acknowledgements

Support from the NSF-STC SAHRA (Sustainability of Semi-Arid Hydrology and Riparian Areas) under Agreement No. EAR-9876800 is gratefully acknowledged. This work would not have been possible without the help and organization of Dave Goodrich and Bruce Goff.

References

- Bevington, P., Robinson, D., 1992. *Data Reduction and Error Analysis for the Physical Sciences*, 2nd Edition. McGraw-Hill, New York, 328 pp.
- Brutsaert, W., 1982. *Evaporation into the Atmosphere*. Reidel, Dordrecht, 299 pp.
- Brutsaert, W., 1998. Land-surface water vapor and sensible heat flux: spatial variability, homogeneity, and measurement. *Water Resour. Res.* 34 (10), 2433–2442.
- Cooney, J., 1970. Remote measurements of atmospheric water vapor profiles using the Raman component of laser backscatter. *J. Appl. Meteorol.* 9 (1), 182–184.
- Cooney, J., Petri, K., Salik, A., 1985. Measurements of high resolution atmospheric water vapor profiles by the use of a solar-blind Raman lidar. *Appl. Opt.* 24 (1), 104–108.
- Cooper, D.I., Eichinger, W.E., Hipps, L., Kao, J., Reisner, J., Smith, S., Schaeffer, S.M., Williams, D.G., 1999. Spatial and temporal properties of water vapor and flux over a riparian canopy. *Agric. For. Meteorol.* 105, 161–183.
- Ehret, G., Kiemle, C., Renger, W., Simmet, G., 1993. Airborne remote sensing of tropospheric water vapor with a near-infrared differential absorption lidar system. *Appl. Opt.* 32 (24), 4534–4551.
- Eichinger, W., Cooper, D., Parlange, M., Katul, G., 1993a. The application of a scanning, water-Raman lidar as a probe of the atmospheric boundary layer. *IEEE Trans. Geosci. Remote Sensing* 31 (1), 70–79.
- Eichinger, W., Cooper, D., Holtkamp, D., Karl Jr., R., Moses, J., Quick, C., Tiede, J., 1993b. Derivation of water vapor fluxes from lidar measurements. *Bound. Layer Met.* 63, 39–64.
- Eichinger, W., Cooper, D., Forman, P., Griegos, J., Osborne, M., Richter, D., Tellier, L., Thornton, R., 1999. The development of a scanning Raman water-vapor lidar for boundary layer and tropospheric observations. *Atm. Oceanic Technology*, 16 (1), 1753–1766.
- Finn, D., Lamb, B., LeClerc, M., Horst, T., 1996. Experimental evaluation of analytical and Lagrangian surface layer flux footprint models. *Bound. Layer Met.* 89, 283–308.
- Higdon, N.S., Browell, E.V., Ponsardin, P., Grossmann, B.E., Butler, C.F., Chyba, T.H., Mayo, M.N., Allen, R.J., Heuser, A.W., Grant, W.B., Ismail, S., Mayor, S.D., Carter, A.F., 1994. Airborne differential absorption lidar system for measurements of atmospheric water vapor and aerosols. *Appl. Opt.* 33, 6422–6438.
- Horst, T., 1999. The footprint for estimation of atmosphere–surface exchange fluxes by profile techniques. *Bound. Layer Met.* 90, 171–188.
- Horst, T., Weil, J., 1994. How far is far enough? The fetch requirements for micrometeorological measurement of surface fluxes. *J. Atmos. Ocean. Tech.* 11, 1018–1024.
- Jackson, R., Moran, S., Gay, L., Raymond, L., 1987. Evaluating evaporation from field crops using airborne radiometry and ground based meteorological information. *Irrigation Sci.* 8, 81–90.
- Kaimal, J., Finnigan, J., 1994. *Atmospheric Boundary Layer Flows*. Oxford University Press, New York, 289 pp.
- LeClerc, M., Thurtell, G., 1990. Footprint prediction of scalar fluxes using a Markovian analysis. *Bound. Layer Met.* 52, 247–258.
- Mahrt, L., 1998. Flux sampling errors for aircraft and towers. *J. Atmos. Ocean. Tech.* 15 (2), 416–429.
- Melfi, S.H., Lawrence, J.D., McCormick, M.P., 1969. Observation of Raman scattering by water vapor in the atmosphere. *Appl. Phys. Lett.* 15 (9), 295–297.
- Nedeljkovic, D., Hauchecorne, A., Chanin, M.L., 1993. Rotational Raman lidar to measure the atmospheric temperature from the ground to 30 km. *IEEE Trans. Geosci. Remote Sensing* 31 (1), 90–101.
- Renault, D., Pournay, C., Capitini, R., 1980. Daytime Raman lidar measurements of water vapor. *Opt. Lett.* 5 (6), 232–235.
- Schaeffer, S.M., Williams, D.G., 1998. Sap flux estimates of transpiration from a cottonwood/willow riparian forest canopy. *Agric. For. Meteorol.* 105, 257–270.
- Stull, R., 1988. *An Introduction to Boundary Layer Meteorology*. Kluwer Academic Publishers, Boston.